



DNS of Turbulent Premixed Ammonia/Hydrogen Flames: The Impact of Thermo-Diffusive Effects

Jessica Gaucherand^{1,2} · Davide Laera^{1,3} · Corinna Schulze-Netzer² · Thierry Poinso^{1,4}

Received: 29 August 2023 / Accepted: 17 November 2023 / Published online: 19 December 2023
© The Author(s) 2023

Abstract

Direct Numerical Simulations (DNS) of three-dimensional premixed turbulent hydrogen-air flames enriched with 19%, 36%, 44% and 57% of NH_3 (in volume) are performed. Starting from an equivalence ratio of 0.44 for the case with 19% of NH_3 , richer mixtures of $\phi = 0.54, 0.69$ and 0.95 are considered when increasing NH_3 concentration to obtain comparable laminar flame speeds, i.e., 0.17 m/s for 19% and 36 % NH_3 enriched case, and 0.30 m/s when NH_3 concentration is increased to 44 and 57%. The composition and characteristics of the studied mixtures enable to investigate the effects of thermo-diffusivity in a turbulent flow and the role of chemistry and stretch effects in the development of the flames. Given a composition of ammonia and hydrogen and an equivalence ratio, a predictive method is described to identify compositions where thermo-diffusive effects impact the flame and predict the stretch factors. Two maps are proposed to achieve this: the first one is based on the Markstein number and the second one is based on the ratio of consumption speed of strained flames over the laminar unstretched flame speed. This prediction can guide model selection and help manufacturers and experimentalists identify relevant operating points based on desired energy output.

Keywords Direct numerical simulation · Premixed turbulent flame · Ammonia · Hydrogen · Thermo-diffusive instabilities

✉ Jessica Gaucherand
gaucherand@cerfacs.fr

¹ CERFACS, 42 Avenue Gaspard Coriolis, 31057 Toulouse, France

² Department of Energy and Process Engineering, Norwegian University of Science and Technology, NO-7034 Trondheim, Norway

³ Department of Mechanics, Mathematics and Management, Polytechnic University of Bari, Via Orabona 4, 70125 Bari, Italy

⁴ IMFT, Allée du Professeur Camille Soula, 31400 Toulouse, France

1 Introduction

Recent interest in decarbonizing energy systems such as gas turbines, internal combustion engines, boilers and furnaces is leading to an interest in utilizing carbon-free fuels such as hydrogen (H_2) or ammonia (NH_3). However, integrating these new fuels into combustors is challenging. For instance, H_2 large flame speed at stoichiometry and wide flammability ranges, not only require potential chamber redesign but also raise safety concerns regarding transportation and storage (Staffell et al. 2019). In contrast, NH_3 is easier to store and transport (MacFarlane et al. 2020) but its major drawback is its low flame speed which limits its direct use in combustion systems. To offset this, researchers have explored the potential of mixing NH_3 with H_2 to find a compromise between each fuel's advantages and drawbacks (Ichikawa et al. 2019; Valera-Medina et al. 2021).

In this context, high fidelity Direct Numerical Simulation (DNS) can be employed in combustion research to investigate the properties of such multi-fuel combustion, supporting the development and validation of combustion models (Rogallo and Moin 1984; Orszag 1970; Domingo and Vervisch 2022). Work on laminar and turbulent premixed combustion of ammonia/hydrogen fuel mixtures has highlighted the importance of thermo-diffusive effects. Indeed, some mixture's thermo-chemical and transport properties will lead to intrinsic instabilities, which are not caused by external sources. Two major types of instabilities can be distinguished: the hydrodynamic instabilities (Darrieus 1938; Landau 1988) and thermo-diffusive instabilities (Barenblatt 1962). The first cause flame speed modulation due to thermal expansion, and are unconditionally destabilizing at any wavelength. The latter stabilizes or destabilizes the flame compared to the hydrodynamic instabilities. Thermo-diffusively unstable mixtures occur at small scales, with sizes close the flame thickness, and are due to a competition between the deficient reactant's diffusivity and the temperature diffusion's speed (Matalon 2007). This can be characterized by the Lewis number: when the deficient reactant is slower than temperature, typically characterized by Lewis number above 1, thermo-diffusive effects are stabilizing. When the deficient reactant is faster than the heat diffusion, which is also called preferential diffusion of light or fast diffusing species, the Lewis number is lower than one and thermo-diffusive effects are destabilizing. Although intrinsic instabilities are understood in the context of laminar flames (Berger et al. 2022; Gaucherand et al. 2023), the investigation of unstable mixtures in turbulent flows is also relevant (Berger et al. 2022). In regards to laminar ammonia and hydrogen mixtures, Wiseman et al. (2021) performed a comparison of numerical and experimental studies of the blowout behavior of a lean ($\phi = 0.45$) turbulent 3-D premixed $NH_3/H_2/N_2$ flame, finding preferential diffusion effects, reaching an increase of the flame speed of two times of an unstretched flame in the same conditions. A large increase of the flame surface area and fuel consumption rate was observed, which was related to hydrogen's preferential diffusion and prevented extinction. DNS of spherically expanding turbulent NH_3/H_2 -air flames with different fuel ratios and equivalence ratios found important distortion due to equivalence ratio local variation, and more wrinkling as H_2 content increased (Mukundakumar and Bastiaans 2022). This study was limited to an equivalence ratio between 0.8 and 1.2. In a study with premixed turbulent flames (Yang et al. 2022) at elevated pressure, stronger wrinkling was found at an equivalence ratio of 0.9 for pure NH_3 and NH_3/H_2 mixtures (with up to 15% of H_2 in the fuel in volume fraction) compared to the rich ($\phi = 1.1$) and stoichiometric mixtures. 2-D and 3-D DNS of turbulent ammonia/hydrogen flames at different pressures have also been performed by Rieth et al. (2022) finding thermo-diffusive effects and local enrichment of positively curved portions of the

flame at $\phi = 0.45$ for a $\text{NH}_3/\text{H}_2/\text{N}_2$ mixture of respectively 40%/45%/15% in volume fraction in the fuel. Another study by the same authors investigated the formation of NO_x with regards to the observed enrichment in turbulent flames (Rieth et al. 2023). NO_x production was also investigated both in laminar and turbulent ammonia/hydrogen flames with 40% of hydrogen at stoichiometry (Karimkashi et al. 2023), where NO production was lower in positive curvature zones, a phenomenon attributed to H_2 preferential diffusion in these zones which was also observed by Netzer et al. in a 2-D laminar study (Netzer et al. 2021) with the same fuel mixture as Rieth et al. but with equivalence ratio from 0.3 to 1.1. Netzer et al. also considered ammonia cracking proportions with 72%/21%/7% of $\text{NH}_3/\text{H}_2/\text{N}_2$. The behavior of lean, unstable, ammonia/hydrogen premixed mixtures does not seem to differ largely from what is known for pure hydrogen flames. Indeed, in pure hydrogen lean flames ($\phi = 0.45$ in Coulon et al. (2023) and 0.4 in Berger et al. (2019)), turbulent premixed simulations have identified flame surface reduction and flame consumption speed increased due to thermo-diffusive effects from hydrogen's preferential diffusion. These results indicate that equivalence ratio and fuel composition affect the development of thermo-diffusive effects. Hydrogen has been investigated both theoretically, numerically and experimentally for a long time (Im and Chen 2002; Lee et al. 2022): preferential diffusion phenomena in hydrogen-premixed flames and specifically lean flames have been discussed in the literature, notably by Matalon (2007) and Lipatnikov and Chomiak (2005). Hochgreb (2023) highlighted in a recent review, the large flame speed laminar and turbulent flame speeds of hydrogen could reach, notably due to the thermo-diffusively unstable nature of these mixtures, and on the need of combustion models to account for the impact these thermo-diffusive effects in these flames. A large number of work has highlighted the need for lean H_2 flames to account for the flame speed increase due to thermo-diffusive effects in combustion model (Berger et al. 2022; Aniello et al. 2022). In the case of NH_3/H_2 mixtures, the same need has been identified (Gaucherand et al. 2023), but the limited mixture composition investigated in the literature (Netzer et al. 2021; Wiseman et al. 2021; Mukundakumar and Bastiaans 2022; Yang et al. 2022; Rieth et al. 2022, 2023; Karimkashi et al. 2023; Coulon et al. 2023) still raises the question of the range of conditions where thermo-diffusive effects impact turbulent flames in ammonia/hydrogen blends, and at which intensity.

In order to investigate the effects of unstable ammonia/hydrogen mixtures in turbulent flows, this article presents four DNS of turbulent premixed NH_3/H_2 flames in a slot burner configuration. The objective of the simulations is twofolds: the first one is to create a database of turbulent premixed NH_3/H_2 flames, with equivalence ratio varying between 0.44 and 0.95, and NH_3 content varying between 19% and 54% in volume. Cases A (19% of NH_3 , $\phi = 0.44$) and B (36% of NH_3 , $\phi = 0.54$) have a similar flame speed, and so do Cases C (44% of NH_3 , $\phi = 0.69$) and D (57% of NH_3 , $\phi = 0.95$). Indeed, ammonia/hydrogen mixtures are notably investigated to phase out carbon-based fuels such as methane in engines. Methane-based engines operate at various load and equivalence ratios, going from very lean to stoichiometric. Therefore, representative conditions of the laminar flame speed of lean methane flames were picked and two target flame speeds were selected: 0.17 m/s which is representative of a lean methane flame of $\phi \approx 0.7$ and a flame speed of 0.30 m/s which is representative of a lean methane flame of $\phi \approx 0.85$. As the two laminar flame speeds are targeted, the equivalence ratio and ammonia/hydrogen fuel content are tuned using two combinations.

The second objective is to study the proposed flames and gain in understanding on their flame structure and response to thermo-diffusive effects. Furthermore, in terms of modeling, questions remain on the appearance of thermo-diffusive effects in NH_3/H_2 flames and the construction of models for flame speed enhancement observed in the DNS flames.

The numerical setup and DNS solver are presented in Sect. 2. Section 3 shows the flame topology and preferential diffusion impact on the flame structure. A predictive method is developed and tested on the DNS to investigate the mixture's tendency to have a stretch factor higher than unity based on the mixture composition and one-dimensional flames. This prediction can guide model selection and help manufacturers and experimentalists identify relevant operating points based on desired energy output.

2 Theory, Numerical Setup and Methodology

2.1 Numerical Solver and Chemistry

In this work, the flow is modeled by the reacting Navier–Stokes equations with the compressible solver AVBP¹ (Schönfeld and Rudgyard 1999), an explicit massively parallel code. A third-order accurate in space and time Taylor-Galerkin finite-element scheme is used for the discretization of the convective terms, while a second-order Galerkin scheme is used for diffusion terms (Colin and Rudgyard 2000).

The flow is gaseous and NH₃/H₂-air chemistry is modeled using an analytically reduced chemistry mechanism which is reduced from CRECK (Stagni et al. 2020) with the in-house software Arcane (Cazères et al. 2021), composing 14 transported species, 7 species with QSS assumption and 88 reactions. Validation of the reduced chemistry is included in the Supplementary Materials. A power law is used to compute the molecular viscosity. Constant Schmidt Sc and Prandtl Pr numbers are used for species molecular diffusion: $D_k = \mu/Sc_k$, for species k , and for thermal conductivity: $\lambda = \mu C_p/Pr$ with C_p the specific heat capacity of the mixture. Pr of 0.7 is selected as it corresponds to the Prandtl number of air, the main component in the premixed mixtures.

2.2 Numerical Set-up and Boundary Conditions

The target configuration corresponds to a turbulent slot burner where burned gases are initiated in the domain and surround fresh gases. Turbulence is injected in the central zone of one-third of the inlet (Fig. 1). The 3-D domains are parallelepiped with dimensions $L_x \times L_y \times L_z$ given in Table 1. The dimensions L_x are chosen based on the estimated flame brush from simulations with a coarser grid (3 points in the flame front). Domains are discretized on regular Cartesian meshes composed of $N_x \times N_y \times N_z$ hexahedral cells of size Δx given in Table 1. Laminar 1-D planar unstretched flames were first computed, initialized with Cantera (Goodwin et al. 2022) solutions, to determine the spatial resolution of species mass fractions, temperature and density profiles and to choose an adequate number of points (N_c) in each thermal thickness δ_L^0 :

$$\delta_L^0 = \frac{T_{ad} - T_u}{\max(\nabla T)}, \quad (1)$$

¹ <http://www.cerfacs.fr/avbp7x>.

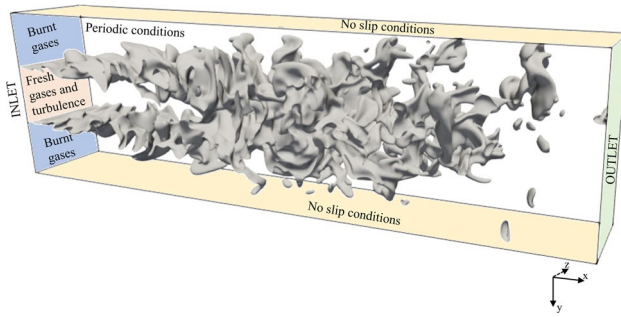


Fig. 1 Set-up of the 3-D DNS simulations. Two coflows of burnt gases of each respective cases surround the injection of fresh gases where turbulence is also injected following a Passot-Pouquet spectrum

Table 1 Parameters and mesh information of the simulations with NH_3 content in volume, equivalence ratio ϕ , laminar flame speed s_l^0 , u'/s_l^0 , l_t/δ_L^0 , Karlovitz number Ka , Reynolds number Re , turbulent Reynolds number Re_t , laminar flame thickness δ_L^0 , cell size Δ_x , numbers of points in thermal thickness N_c , lengths in x , y and z direction L_x, L_y, L_z , and numbers of points in x , y and z direction N_x, N_y, N_z

Case name	A	B	C	D
X_{NH_3} [%]	19	36	44	57
ϕ [-]	0.44	0.54	0.69	0.95
s_l^0 [m/s]	0.17	0.17	0.30	0.30
u'/s_l^0 [-]	14.7	14.7	8.3	8.3
l_t/δ_L^0 [-]	3.03	3.35	4.26	4.16
Ka [-]	32	31	11.6	11.8
Re [-]	12 597	12 594	12 384	12 155
Re_t [-]	617	617	610	603
δ_L^0 [μm]	705	636	500	513
Δ_x [μm]	38	38	38	41
N_c [-]	18.5	16.8	13	12.5
L_x/H [-]	8.4	7.5	7.8	10.5
L_y/H [-]	3	3	3	3
L_z/H [-]	1.5	1.5	1.5	1.5
N_x [-]	1883	1693	1744	2191
N_y [-]	673	677	497	671
N_z [-]	337	339	249	336

where T_u is the initial flame temperature (300K), and T_{ad} is the adiabatic flame temperature. The flames are computed at atmospheric pressure. At least 12 points are ensured in the flame front.

The injection of turbulence at the inlet corresponds to homogeneous and isotropic turbulence using a Passot-Pouquet turbulence spectrum (Passot and Pouquet 1987) where the turbulent intensity u' corresponds to 10% of the bulk velocity ($U_{bulk} = 25$ m/s) injected in the central slot. For the details regarding the generation of turbulence through a Fourier series decomposition, readers are referred to Kraichnan (Kraichnan 1970). The spectra decay slowly over time and more details are presented in the Supplementary Materials. A smooth transition from U_{bulk} to U_{coflow} is enforced through a hyperbolic tangent function between the central fresh gas jet and the burnt gas coflow surrounding it. The domain is periodic in the spanwise direction (z), no-slip conditions are specified in the

crosswise direction (y) and static pressure is imposed at the outlet. Both inlet and outlet boundary conditions are treated with the Navier–Stokes Characteristic Boundary Conditions (NSCBC) (Poinsot and Lele 1992). More details for the description of the setup, and information on turbulent injection and shear turbulence development, can be found in Coulon et al. (2023) and is reported in the Supplementary Materials. Table 1 presents the parameters of the four 3-D simulations performed, with the NH_3 content in volume, equivalence ratio ϕ , u'/s_L^0 , l_t/δ_L^0 , which are needed in order to compute Karlovitz number $\text{Ka} = (l_t/\delta_L^0)^{-1/2}(u'/s_L^0)^{3/2}$, Reynolds number $Re = U_{\text{bulk}}H/\nu$, where ν is the kinematic viscosity of the mixture, the turbulent Reynolds number $Re_t = u'l_t/\nu_u$, the laminar flame thickness δ_L^0 , cell size Δ_x , numbers of points in thermal thickness $N_c = \delta_L^0/\Delta_x$, lengths in x , y and z direction L_x , L_y , L_z , and numbers of points in x , y and z direction N_x , N_y , N_z . With H the height of the central jet, corresponding to one-third of L_y . l_t is the integral length scale of the turbulence spectrum, corresponding to one-fourth of H (Poinsot and Veynante 2005; Domingo and Vervisch 2022). The four flames are situated in the thin reaction zone defined by the Borghi–Peters diagram (Borghi 1985; Peters 2000) which is presented in the Supplementary Materials. The simulations are performed during two flow-through times.

3 Results and Discussion

3.1 Premixed Turbulent NH_3/H_2 -air Flames

Figure 2 displays snapshots of heat release rate normalized by the maximum heat release rate of the 1-D unstretched flame for the four flames after two flow-through times at a cut in the z -axis. Figure 3 presents the contour of local equivalence ratio ϕ minus the initial equivalence ratio in the fresh gases.² This normalization is to visualize the effects of preferential diffusion on the flame: the equivalence ratio found in the turbulent flame brush reaches larger (as well as lower) values than the injected equivalence ratio when preferential diffusion becomes significant.

A shorter flame brush length is captured for leaner cases (A, B and C). Zones of high heat release rate are captured along the flame front for all cases. In Case A, for example, the heat release rate in the 3-D DNS is up to five times higher than the maximum heat release rate of the equivalent unstretched laminar case. Strong variations of the equivalence ratio are also seen in all cases. The following sections detail these observations.

² The local equivalence ratio ϕ is defined using the elemental mass fraction of atomic hydrogen Z_H and of atomic oxygen Z_O :

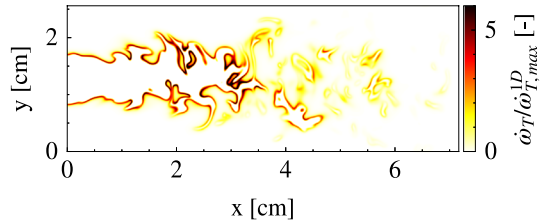
$$\phi = \frac{Z_H/Z_0}{(Z_{H,u}/Z_{O,st})}, \quad (2)$$

with u indicating the fresh mixture and st the stoichiometry and with:

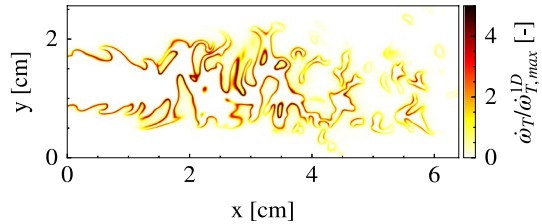
$$Z_i = \sum_{j=1}^S \mu_{ij} Y_j, \quad (3)$$

where i is either H or O , S is the total number of species in the chemical scheme, j is the species, and μ_{ij} is the mass proportion of i in j .

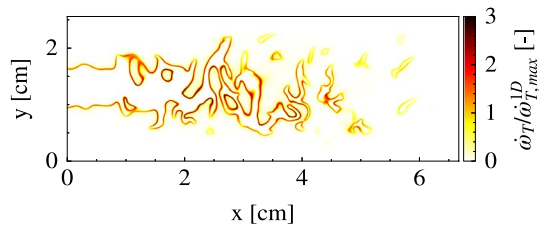
Fig. 2 Contour of heat release rate normalized by the maximum heat release rate of the unstretched flames for the four flames after two flow-through times at a cut in the center of the z-axis



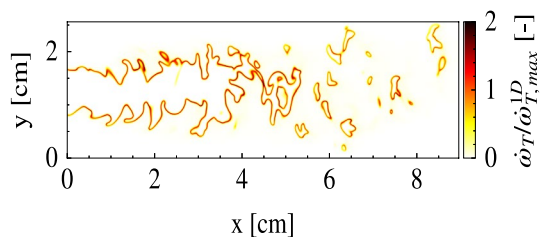
(a) Case A (19% of NH_3 , $\phi = 0.44$)



(b) Case B (36% of NH_3 , $\phi = 0.54$)



(c) Case C (44% of NH_3 , $\phi = 0.69$)

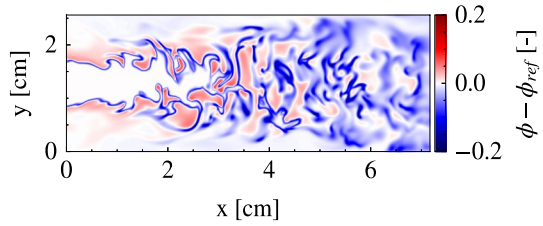


(d) Case D (57% of NH_3 , $\phi = 0.95$)

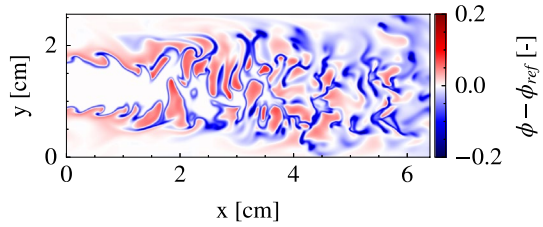
3.1.1 Progress Variable Definition

The combustion process of NH_3/H_2 mixtures needs to be parameterized using an appropriate definition of the progress variable. A modeling strategy to characterize preferential diffusion effects is the use of two controlling variables to parameterize the scatter of the mixture. This has been established for different fuels such as hydrogen (Berger et al. 2022; Böttler et al. 2023), methane (Oijen et al. 2010; Kuenne et al. 2011) or syngas (Zhang et al.

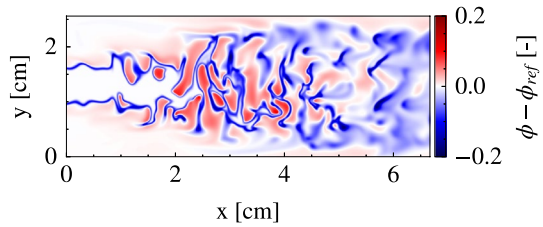
Fig. 3 Contour of equivalence ratio minus the initial equivalence ratio in the fresh gases for the four flames after two flow-through times at a cut in the center of the z -axis



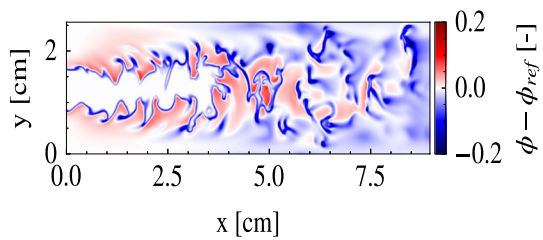
(a) Case A (19% of NH_3 , $\phi = 0.44$)



(b) Case B (36% of NH_3 , $\phi = 0.54$)



(c) Case C (44% of NH_3 , $\phi = 0.69$)



(d) Case D (57% of NH_3 , $\phi = 0.95$)

2021) exhibiting preferential diffusion effects. The following two controlling variables are commonly used:

- a progress variable c ,
- a mixture fraction Z .

The definition of the mixture fraction is well established, and the Bilger’s expression is used (Bilger et al. 1990). However, an appropriate progress variable definition in the case of ammonia/hydrogen needs to be defined. Furthermore, many modeling strategies rely on tabulation and the thermochemistry of the reacting flow from burn to unburned gas can be mapped in the composition space described by the combination of progress variable and mixture fraction. Two constraints are imposed on the progress variable: a monotonous growth from fresh ($c = 0$) to burn gas ($c = 1$) to uniquely describe each thermochemical state and the thermochemical variables should vary at a moderate speed with the progress variable, since, if not verified, it would mean a small deviation in c would result in large errors in the thermochemical variables (Ihme et al. 2012; Niu et al. 2013; Prüfert et al. 2015). Typical definitions for the progress variable are based on enthalpy (E), temperature (T), density (ρ), one species or a combination of several species. Recent work involving mixtures of ammonia and hydrogen have proposed H_2O (Rieth et al. 2023; Wiseman et al. 2021; Mukundakumar and Bastiaans 2022; Netzer et al. 2021) as the progress variable, a combination of products $H_2O/NO/NO_2$ (Chi et al. 2023), or temperature (Karimkashi et al. 2023). Other studies focusing on pure hydrogen have investigated the use of H_2 or H_2O to describe the scatter of heat release rate obtained for turbulent 3-D DNS (Berger et al. 2022) and for, initially laminar, perturbed 2-D DNS (Berger et al. 2022). The database of the four 3-D DNS NH_3/H_2 -air flames is at first used to select the most suitable progress variable c that would reduce the error in describing the scatter of important parameters Q such as heat release rate $\dot{\omega}_T$ and equivalence ratio ϕ . Given a quantity Q , an irreducible error ϵ_{irr}^2 can be defined as:

$$\epsilon_{irr}^2 = \langle (Q - \langle Q | c \rangle)^2 \rangle, \tag{4}$$

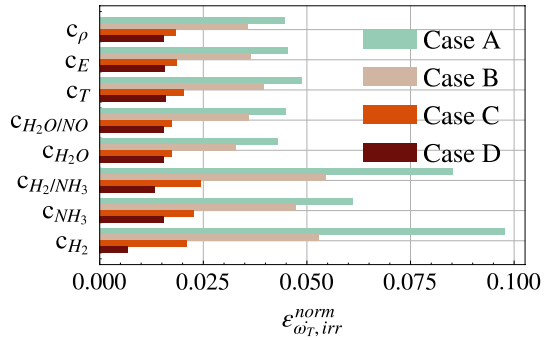
where $\langle \rangle$ is an ensemble average and $\langle Q | c \rangle$ is the conditional mean of Q with respect to c . To compare the different cases, Eq. (4) is normalized. For the heat release rate, the normalization is done with respect to the maximum heat release of an unstretched flame of the same composition:

$$\epsilon_{\dot{\omega}_T, irr}^{norm} = \frac{\epsilon_{irr}^2}{\max(\dot{\omega}_T^{1-D})^2}. \tag{5}$$

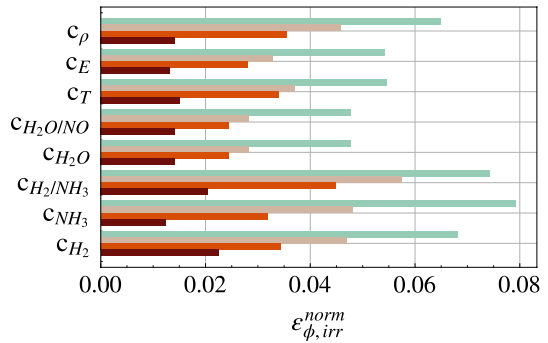
Similarly, for the local equivalence ratio, $\epsilon_{\phi, irr}^{norm}$ is normalized with the global equivalence ratio of the fresh gases. The maximum value of the irreducible error is computed, and the smallest value between the different progress variable definitions indicates that the target quantity Q is well characterized by the parameter c (Berger et al. 2022). Different progress variable definitions found in literature (Rieth et al. 2023; Berger et al. 2022; Chi et al. 2023; Oijen et al. 2010; Lehtiniemi et al. 2006; Pierce and Moin 2004; Knop et al. 2011) are tested:

- $c_{H_2} = 1 - \frac{Y_{H_2}}{Y_{H_2,u}}$,
- $c_{NH_3} = 1 - \frac{Y_{NH_3}}{Y_{NH_3,u}}$,
- $c_{H_2/NH_3} = 1 - \left(X_{H_2} \frac{Y_{H_2}}{Y_{H_2,u}} + X_{NH_3} \frac{Y_{NH_3}}{Y_{NH_3,u}} \right)$,
- $c_{H_2O} = \frac{Y_{H_2O}}{Y_{H_2O,b}}$,
- $c_{H_2O/NO} = \frac{Y_{H_2O} - Y_{NO}}{Y_{H_2O,b} - Y_{NO,b}}$,

Fig. 4 Maximum irreducible error of the heat release rate $\dot{\omega}_T$ (top) and the local equivalence ratio ϕ (bottom) for different progress variable definitions for the four cases. c_{H_2O} appears as a good candidate to be used for describing the heat release rate and local equivalence ratio as it reduces the maximum irreducible error for most cases



(a) Heat release rate $\dot{\omega}_T$



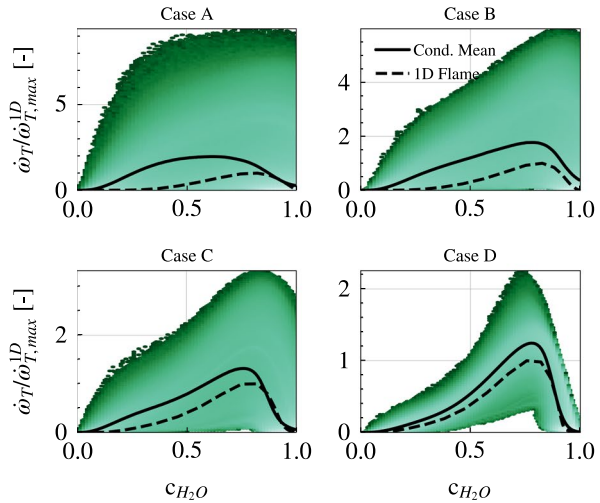
(b) Equivalence ratio ϕ

- $c_T = \frac{T - T_u}{T_{eq} - T_u}$,
- $c_\rho = \frac{\rho - \rho_u}{\rho_{eq} - \rho_u}$,
- $c_E = \frac{E - E_u}{E_{eq} - E_u}$,

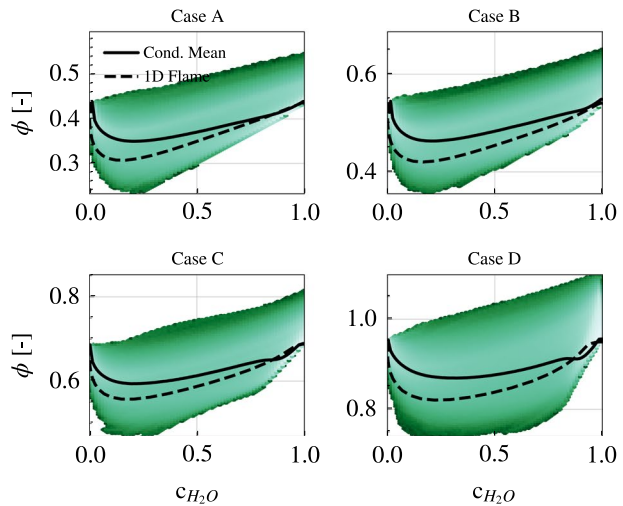
with subscripts b , u , and eq indicating burned, unburned and the equilibrium quantities, respectively. These values were computed using one-dimensional unstretched flames with Cantera. The maximum irreducible errors for $\dot{\omega}_T$ and ϕ computed using each definition of c are reported in Fig. 4a and b. In Cases A, B and C, the smallest error for both the heat release rate and the equivalence ratio is found using c_{H_2O} meaning these target quantities are best parameterized using this progress variable. For Case D, c_{H_2} minimizes the error for the heat release rate but causes the largest error to parameterize the equivalence ratio. The other progress variables give similar error levels for both the heat release rate and local equivalence ratio. Overall, c_{H_2O} appears as a good candidate to be used for describing the two quantities of interest and, therefore, is retained in the rest of this study as the progress variable definition.

The large variations of equivalence ratio and heat release rate observed in Figs. 2 and 3 are illustrated in the progress variable space using c_{H_2O} in Fig. 5. The joint probability density functions of these quantities are also reported together with their conditional mean conditioned by the progress variable (black continuous line). The results are compared to the one of 1-D unstretched flame (black dashed line). A very broad distribution is observed for both quantities. In Fig. 5a, Case A exhibits the largest distribution of heat

Fig. 5 Normalized heat release rate (top) and equivalence ratio (bottom) after two flow-through times with the corresponding joint probability density function of the quantity conditioned by the progress variable c_{H_2O} for the four cases. A lighter shade in the colormap represents a greater probability of the PDF. The dashed line corresponds to the 1-D unstretched laminar flames and the solid line corresponds to the conditional mean of the quantity versus progress variable



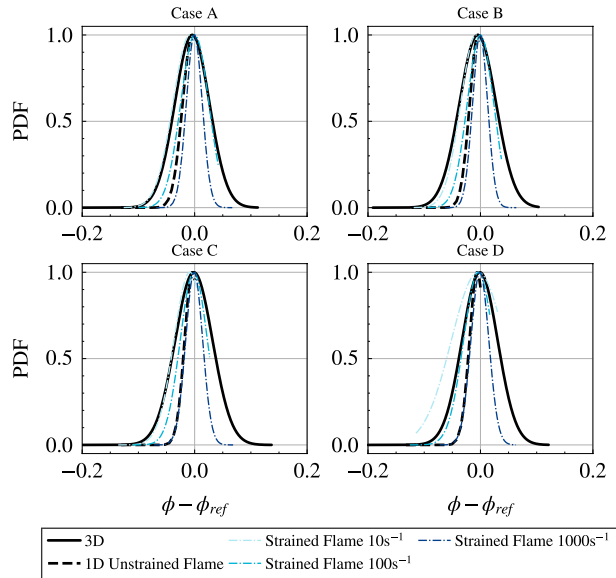
(a) Heat release rate $\dot{\omega}_T$



(b) Equivalence ratio ϕ

release rate, with values of more than 5 times the maximum heat release computed in the 1-D unstretched case. This diminishes with increasing NH_3 concentration (Case A to D) to only two times the maximum one of its unstretched counterpart. Regarding the comparison with the unstretched flame and the conditional mean of the 3-D case, a large deviation is obtained for Case B over the whole range of the progress variable. For Cases A, C and D however, the deviation is largest for progress variable values up to the maximal heat release rate ($c_{H_2O} \approx 0.8$). At $c > 0.8$, the 1-D unstretched case and the conditional mean are superimposed. The deviation from the conditional mean to the 1-D unstretched results of heat release rate are strongest for Case A and declines with increasing equivalence ratio to Case

Fig. 6 PDF of equivalence ratio minus the reference equivalence ratio over the whole domain for the four cases. Comparison with strained twin flames computed with Cantera (10, 100 and 1000 s^{-1}) and the unstrained flame. Each PDF was normalized by its maximum values to compare the results



D. Similar results have been found by Wiseman et al. (2021) where a broad distribution of the heat release rate and a deviation of the conditional mean from the unstrained flame was found for a case with 40% NH_3 , 45% H_2 , and 15% N_2 in the fuel blend and an equivalence ratio of 0.45. The deviation was attributed to large values of strain. Similar results have also been found for lean pure H_2 flames (Berger et al. 2022; Coulon et al. 2023; Song et al. 2022; Rieth et al. 2022).

Regarding the equivalence ratio (Fig. 5b), a broad distribution of values is found around the initially imposed equivalence ratio of the fresh gases ϕ_{ref} . The conditional mean and 1-D results are the same in the fresh and burned gas corresponding to the initial equivalence ratio imposed. In the region in-between, a deviation between the conditional mean and 1-D flame is found: the turbulence affects the inner flame front, causing overall enrichment compared to its 1-D counterpart. The broad distribution of the equivalence ratio indicates preferential diffusion enriching and making the mixture leaner in different places. The probability density function of the equivalence ratio minus the fresh gas equivalence ratio (Fig. 6) informs that all 3D cases have a distribution of equivalence ratio between $\phi_{ref} - 0.2$ and $\phi_{ref} + 0.1$ and indicates preferential diffusion for the four cases. Compared to the unstrained flames (dashed lines), for which the equivalence ratio is never richer than the global one, the strained 1-D flames (dotted-dashed lines), computed using the twin flame configuration in Cantera, exhibit enrichment. Therefore, these strained elements are responsible for the enrichment in the 3D cases: In Cases A and B, low strain values (10 s^{-1}) match the 3-D lean side, and higher strain values (1000 s^{-1}) match the 3-D rich side PDF. For Cases C and D, the lean side is matched by low strain values (10 s^{-1} for C and (100 s^{-1} for D). We don't see a match for the whole range of the PDF on the rich side, but we expect intermediate strain values to match them. The turbulence interacts with the flame and leads to strained flame elements for which the equivalence ratio varies strongly. The impact of the strained elements on the heat release rate of the different cases is investigated later. Finally, the enrichment due to focusing in curved region should not be neglected and also contributes to the overall change in equivalence ratio. A study by (Aspden et al. 2015)

tested different transport hypothesis to compare the Lewis number effects (species diffusion vs thermal diffusion) but also the preferential diffusion effects (fuel diffusion vs oxidizer diffusion). In this study, these effects are not separated but are of interest to consider in further study, especially considering the multi-fuel aspect.

3.1.2 Stretch Factor

Another way to estimate the flamelet deviation of lean ammonia/hydrogen mixtures is to compute the stretch factor I_0 , which accounts for the influence of stretch and measures the deviation between the increase of flame area due to wrinkling and the turbulent flame speed:

$$I_0 = \frac{\Omega^*}{s_L^0} \frac{1}{A_T}, \quad (6)$$

with s_L^0 the unstretched laminar flame speed and A_T , the turbulent flame surface. The total reaction rate Ω^* is:

$$\Omega^* = -\frac{1}{\rho_u Y_{f,u}} \int_V \dot{\omega}_f dV, \quad (7)$$

is a normalized total volumetric burning rate over the whole volume V . ρ_u is the density of the fresh gases, $Y_{f,u}$, the initial mass fraction of fuel in the mixture, and $\dot{\omega}_f$ is the fuel's reaction rate. Due to the presence of two fuels in the mixture (H_2 and NH_3), Ω^* is computed using both fuels so that a stretch factor for each fuel I_{0,NH_3} and I_{0,H_2} can be defined. The turbulent flame surface A_T is computed by integrating the flame surface density over the whole flame:

$$A_T = \int_V |\nabla c_{H_2,0}| dV. \quad (8)$$

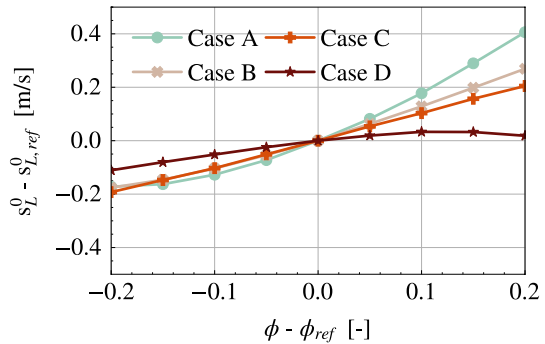
Similar turbulent flame surfaces are obtained for the four different flames, despite shorter flame brush lengths for Cases A, B and C (Figs. 2, 8). This indicates that Cases A, B and C are more wrinkled. Time-averaged values during the second flow-through time of the stretch factors are reported in Table 2.

Very similar values are found for Cases A, B and C regardless of the fuel considered in Eq. (7). In Case D, the difference between I_{0,NH_3} and I_{0,H_2} is due to the production of H_2 by NH_3 as will be seen in the following section. As anticipated from Fig. 5, the stretch factor diminishes from Case A to Case D. In Case A values of I_0 close to 3 are obtained, indicating that each surface element of the flame front can burn almost 3 times more than the laminar reference flame as a result of the combined effects of turbulence and thermo-diffusive effects. In Case D, I_0 is close to unity, which indicates that the increase in the turbulent flame speed is only due to the increase of the flame surface and that combustion in the flame brush proceeds almost as the reference flamelet.

In all Cases, H_2 and H notably have very small Lewis numbers and will diffuse faster, leading to preferential diffusion and to the large scatter of equivalence ratio (Fig. 5b). However, since the global initial equivalence ratio (and by extension, the mixture's global Lewis number) in the fresh gas differs for each case, the impact on

Table 2 Stretch factor values for the four cases using the reaction rate of NH_3 and of H_2

Case	I_{0,NH_3}	I_{0,H_2}
A	2.69	2.69
B	2.14	2.16
C	1.54	1.52
D	1.29	1.12

Fig. 7 Absolute change of laminar flame speed for equivalence ratio around the reference equivalence ratio of ± 0.2 , which covers the range of equivalence ratio scatter obtained from the 3-D DNS results

heat release rate distribution and stretch factor is different. Case D is close to stoichiometry: the distribution of equivalence ratio due to preferential diffusion is between 0.75 and 1.1. The consumption speed in this range of equivalence ratio in a 1-D unstretched flame reaches a plateau since the local initial equivalence ratio is around stoichiometry. This observation could explain why the conditional mean of heat release rate (Fig. 5a) is closer to the 1-D unstretched flame, and why the stretch factor is close to unity. Figure 7 shows the absolute change of laminar flame speed for the different mixtures of fuel at different equivalence ratios, with ϕ_{ref} being the reference equivalence ratio at which the 3-D DNS are initialized. The gradient of flame speed increase is strongest for the leanest case, Case A, and is less steep for Cases B, C and D in that same order. Case D's flame speed is, as mentioned, reaching a plateau at around $\phi - \phi_{ref} = 0.1$. Hence, despite similar flame speeds of Cases A and B and of Cases C and D, each Cases' stretch factors are different due to the variation of equivalence ratio and fuel content.

Other works have found similar values of stretch factors close to 2 for lean ammonia/hydrogen/nitrogen mixtures with an equivalence ratio of 0.45 (Wiseman et al. 2021). For pure H_2 , values between 1 and 4 have been found in the literature depending on the equivalence ratio and pressure (Song et al. 2022; Berger et al. 2022; Howarth and Aspden 2022). Our data come as supplemental information to the values of stretch factor ammonia/hydrogen can reach and shows that they can be quite large ($I_0 > 2$).

Fig. 8 Fuel consumption of NH₃ and H₂ for the four cases along the streamwise axis

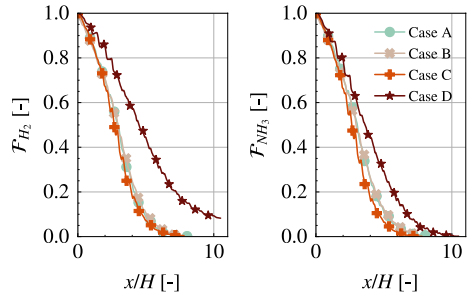
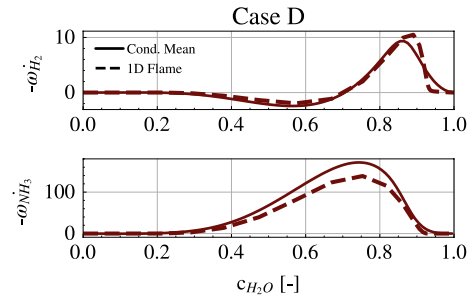


Fig. 9 Reaction rate in kg/s/m³ of 1-D unstretched flame and conditional mean of 3-D cases for H₂ and NH₃ for the four cases along the progress variable space



3.1.3 Fuel Flux and Reaction Rate

The fuel flux along the axial direction can be computed as:

$$\mathcal{F} = \frac{1}{\rho_u U H Y_{f,u}} \int \langle \rho u_x Y_f \rangle dy, \tag{9}$$

where $\langle \rangle$ is the time average during the second flow-through time, U is the bulk velocity, H is the slot size and u_x is the axial velocity. Figure 8 shows the fuel consumption \mathcal{F} along the normalized x -axis for the four cases. Case A, B and C consume both fuels (NH₃ and H₂) faster than Case D: the flame brush is similar for Cases A, B and C, and longer for Case D. Furthermore, for Case D, NH₃ is fully consumed by the domain exit, whereas unburned H₂ still remains. Indeed, Case D is nearly stoichiometric, and local enrichment from preferential diffusion leads to limited O₂ as rich local zones appear, and H₂ is produced by NH₃. This is further illustrated by the reaction rate of the two species in Fig. 9 where $-\dot{\omega}_f$ is illustrated with f being ammonia and hydrogen. A negative value of $\dot{\omega}_f$ corresponds to fuel consumption, while a positive one corresponds to fuel production. Only Case D is presented here as relevant to the current discussion: between $0.4 \leq c \leq 0.6$, H₂ is being produced in non-negligible quantities, due to favorable conditions in terms of fuel proportion and temperature for NH₃ to dissociate into H₂ (Fig. 9). This production is not obtained for the other cases as presented in the Supplementary Material. These results prove that a surplus of hydrogen due to ammonia decomposing into H₂ at moderately high temperatures has a non-negligible effect in Case D explaining why the stretch factor computed with ammonia differs from the one computed with hydrogen (Table 2).

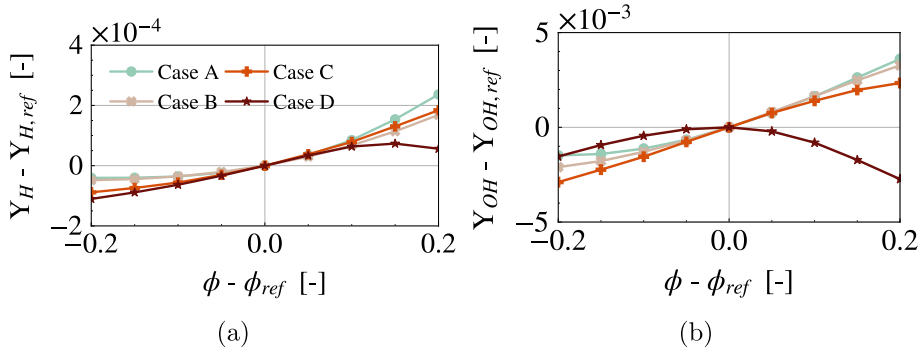


Fig. 10 Absolute change of the maximum mass fraction of different species of 1-D unstretched flames at varying equivalence ratios using the equivalence ratio at which the 3-D DNS were performed as the reference value

3.1.4 Radical Pool

Chemistry effects influence the stretch factor value: light-diffusing species such as H_2 are expected to impact the stretch factor and the resulting heat release rate to be scattered due to preferential diffusion. The impact of intermediate species on preferential diffusion is also worth investigating. Therefore, with the fuel content from the different cases, using 1-D unstretched flame simulations performed using Cantera, the maximum value of the species at different equivalence ratios is computed, as well as the absolute change of the mass fraction, using the equivalence ratio at which the DNSs have been performed as the reference value. The range of equivalence ratios is selected to be somewhat representative of the scatter of equivalence ratio found in the 3-D DNS, where the equivalence ratio is at least around ± 0.2 of the reference value. In the Supplemental Materials, the results for the transported species are presented with the exception of the oxidizer species. Here the focus is on two species with a Lewis number lower than unity, i.e., H and OH. The results are presented in Fig. 10, for the H mass fraction, the mixtures for Cases A, B and C increase around the reference value. The increase of H in Case A for $\phi > \phi_{ref}$ is notably steep. For Case D, the peak of the mass fraction is reached for $\phi - \phi_{ref} = 0.15$, decreasing after this value. The mass fraction of OH increases for the equivalence ratio range for Cases A and B. The evolution of OH for Case C when $\phi > \phi_{ref}$ is slightly less steep than for Cases A and B, but nevertheless increases throughout the range of equivalence ratio investigated. For Case D, the reference equivalence ratio corresponds to where the peak OH production is obtained, meaning a plateau is obtained around this value. The overall increase of light diffusive intermediate species in Cases A, B and C with equivalence ratio contributes to the scatter of heat release rate and equivalence ratio obtained in the 3-D simulations in Figs. 2, 3 and 5. The H radical production and OH production, as local enrichment occurs in the lean Cases A, B and C, illustrate the preferential diffusion effects that affect the 3-D flames. As H and OH increase in the rich, positively curved zones, the consumption speed increases, and the global stretch factor is larger than unity, which indicates that these zones are dominating the flame. On the other hand, the plateau obtained for the production of intermediate species in Case D, either at the reference equivalence ratio, or slightly above is contributing to the attenuated effect of preferential diffusion in 3-D on the scatter of ϕ and ω_T and the stretch factor close to unity of Case D.

This indicates the mixture’s role in an unstable mixture’s development as the initial equivalence ratio and mixture composition dictate preferential diffusion effects. This further motivates the need for a predictive tool based on the initial equivalence ratio and mixture composition to predict the expected consumption speed and heat release rate increase. However, the flow’s influence on the flame and interaction with the unstable mixture is also noteworthy for investigation and will be looked at in the next section by evaluating the strain and curvature.

3.1.5 Strain and Curvature

The total stretch of the flame K is defined as the sum of the tangential strain rate, K_s , and the curvature-induced propagation rate K_c (Poinsot and Veynante 2005):

$$K = K_s + K_c, \tag{10}$$

$$K_c = \kappa s_d, \tag{11}$$

$$K_s = \nabla \cdot \mathbf{u} - \mathbf{nn} : \nabla \mathbf{u}, \tag{12}$$

where $\kappa = \nabla \cdot \mathbf{n}$ is the curvature, \mathbf{u} is the gas velocity and $\mathbf{n} = -\nabla c / |\nabla c|$ is the normal vector to the flame front pointing towards the fresh gases. Positive (negative) curvature elements are convex (concave) towards the burned gases. s_d is the displacement speed, which is the flame front speed relative to the flow (Poinsot and Veynante 2005; Pope 1988) $s_d = (\mathbf{w} - \mathbf{u}) \cdot \mathbf{n}$, or it can also be computed as:

$$s_d = \frac{1}{|\nabla c|} \left(\frac{\partial c}{\partial t} + \mathbf{u} \cdot \nabla c \right). \tag{13}$$

The energy equation can also be used to solve s_d on an isocontour of the progress variable. Typically, the value of the progress variable selected is the one where the heat release rate is maximum in the unstretched flame, indicated as c^* and is case dependent. The values of c^* in the study are the following for Cases A, B, C to D respectively: 0.71, 0.76, 0.76, 0.81. s_d is determined with the heat and species diffusive fluxes and the heat release rates on the isosurface of c^* using the following relation (Poinsot and Veynante 2005):

$$s_d = \underbrace{\frac{1}{\rho C_p |\nabla T|} \left[\nabla \cdot (\lambda \nabla T) + \rho \nabla T \cdot \sum_k (\mathcal{D}_k C_{p,k} \nabla Y_k) \right]}_{S_{d,diff}} + \underbrace{\frac{1}{\rho C_p |\nabla T|} \left(- \sum_k h_k \dot{\omega}_k \right)}_{S_{d,rec}}, \tag{14}$$

where \mathcal{D}_k is the molecular diffusion coefficient, $C_{p,k}$ is the mass-specific heat capacity, Y_k is the mass fraction, h_k is the enthalpy and $\dot{\omega}_k$ is the mass-production rate for the k^{th} species. Therefore, the displacement speed is a net balance between the reaction rates and diffusive fluxes. The latter can be decomposed into a normal component which is generally oriented in the opposite direction to the normal vector \mathbf{n} as defined above, and a tangential component which varies linearly with opposite curvature (Gran et al. 1996; Echehki and Chen 1999). In a steady, unstretched planar laminar flame, the sum of the contribution due to reaction and normal diffusion would be equal to s_L^0 (Peters et al. 1998).

The surface average of a target quantity Q can be computed as:

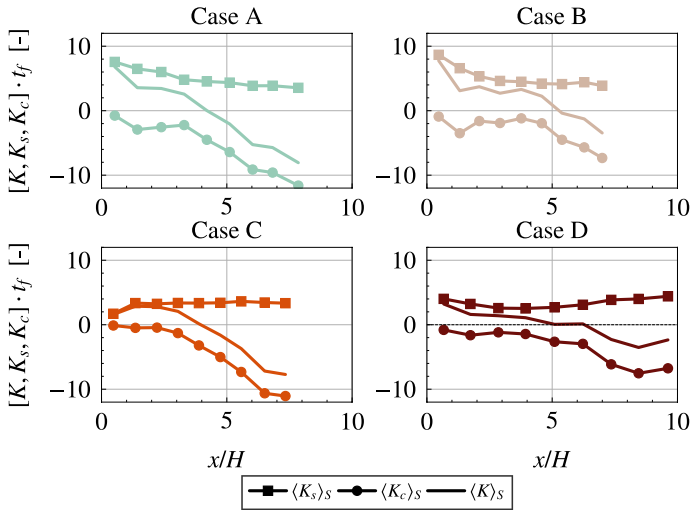
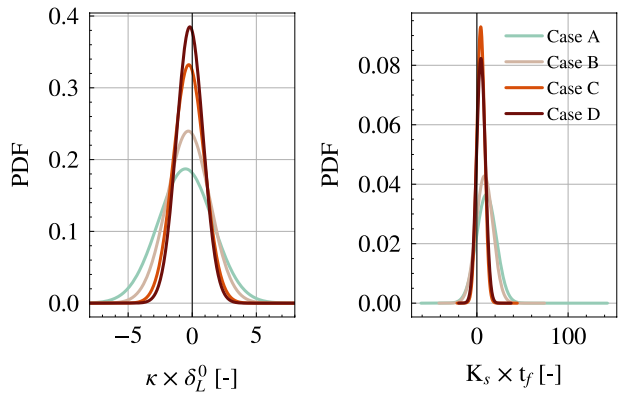


Fig. 11 Surface average of stretch K and stretch components (tangential strain rate K_s , curvature-induced propagation rate K_c) along the x -axis of the four DNS cases, normalized by the flame time of each flame ($t_f = \delta_L^0/s_L^0$)

Fig. 12 Probability density function of normalized curvature and tangential strain rate for the four DNS cases

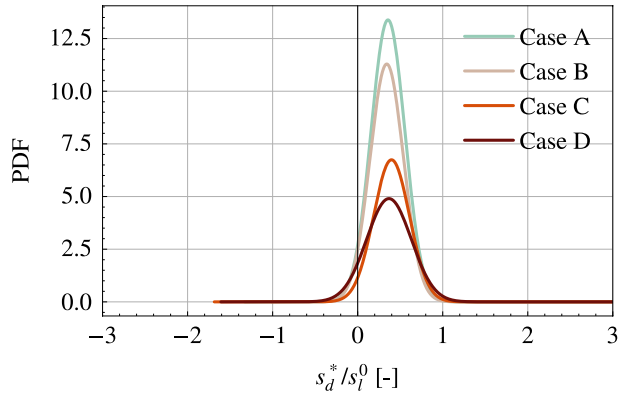


$$\langle Q \rangle_s = \frac{\langle Q |\nabla c| | c^* \rangle}{\langle |\nabla c| | c^* \rangle}, \tag{15}$$

where $\langle \dots | c^* \rangle$ is the conditional average with respect to the isosurface defining the flame front.

The surface averaged mean values of stretch, tangential strain rate and curvature term for the four cases are presented in Fig. 11 using Eq. (14) for s_d . Figure 12 shows the probability density function (PDF) of strain and curvature, normalized, respectively, by τ and δ_L^0 on the same isocontour of progress variable as the surface averaged quantities. The surface averaged curvature-induced propagation rate is negative throughout the flame sheet, whereas the strain-induced rate is positive. This indicates that $\langle K_c \rangle_s$ is responsible for flame surface destruction whereas $\langle K_s \rangle_s$ is responsible for flame surface production in the mean.

Fig. 13 Probability density function of density-weighted displacement speed normalized by s_L^0 for the four DNS cases



Positive values of $\langle K_s \rangle_S$ indicate that the flame surface is more stretched than compressed, as confirmed by the PDF of strain in Fig. 12 where the mean value is positive for the four DNS. The tangential strain is piloted by the turbulent flow field as illustrated from the four Cases in Fig. 11, where Cases A and B have a very similar profile of tangential strain surface average and Cases C and D have a similar profile as well, but lower than the one of A and B. Indeed, the laminar flame speed of these cases (A with B, and C with D) are close, and since the same turbulent profile is injected, this indicates that similar turbulence intensity and scales are perceived by A and B, and by C and D. The surface-averaged curvature rate of the four cases does not follow this same trend, where the four cases have a similar profile in $x/H < 3.5$, then after which cases A and C have a similar profile until the end of the flames. The surface-averaged curvature rate of cases B and D is similar until $x/H = 5$ after which they diverge with $\langle K_c \rangle_S$ of Case D being larger. This indicates curvature's influence by both preferential diffusion phenomena and turbulence. Finally, the surface averaged stretch propagation is controlled for each case, in the first part of the flame, by the tangential strain rate term, and then by the curvature rate term, as the sign of stretch changes from positive to negative. This is due to negative curvature dominating the last end of the flame where the flame is strongly curved and flame bits separate from the flame brush, leading to flame destruction. Similar results have been described for methane (Luca et al. 2019), hydrogen (Coulon et al. 2023; Berger et al. 2022) and hydrogen/ammonia flames (Coulon et al. 2023), and we redirect the reader to these publications for further details on tangential strain and curvature impact on the displacement speed deviation from the unstrained flame speed. In Fig. 13, the density-weighted displacement speed $s_d^* = s_d \rho / \rho_u$ on the iso-surface of progress variable c^* and normalized by the unstretched laminar flame speed of each flame is presented. The positive values indicate that the iso-surface of c^* is moving toward the fresh gases, while the negative values indicate that the iso-surface moves toward the burnt gases. For all cases, the PDF indicates that the iso-surface mainly moves toward the fresh gases. In Fig. 12, the normalized strain PDF of Cases A and B is very close due to their similar laminar flame speed, although the tail of Case A is wider in the positive values especially. Case C and D also have similar PDF of strain profiles, again due to their similar laminar flame speed. The curvature PDF varies with the mean increasing from Case A to D with a wider PDF for Case A.

As known from literature, positively curved zones will be more enriched than negative ones (Berger et al. 2022; Netzer et al. 2021) in flames with species with Lewis numbers lower than one, leading to the broad equivalence ratio found in Fig. 5b which is due to

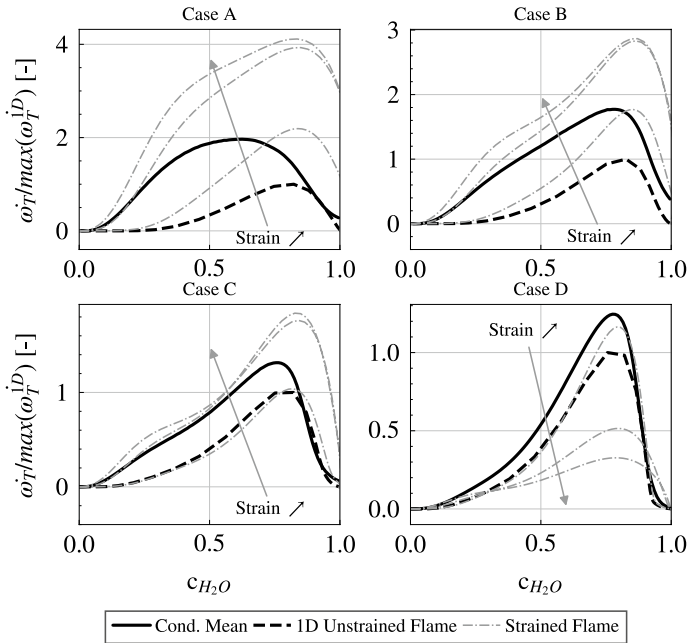


Fig. 14 Heat release rate of 1-D strained twin flames (10 , 100 and 1000 s^{-1}) compared with the conditional mean of the 3-D DNS and the unstretched flame

both the flow structure and the preferential diffusion. However flat flame regions with null curvature also contribute to the deviation from flamelet behavior and lead to higher than unity stretch factor. A recent study (Howarth et al. 2023) has highlighted that flat flame elements are heated after a leading point has passed where preferential diffusion has enhanced the heat release rate and the flame has propagated faster and hotter. The flat flame after the leading point has passed is superadiabatic, which has a higher heat release rate than the unstretched flame. This indicates that both strongly curved elements and flat strained elements contribute to a high heat release rate. To illustrate the effect of strain on heat release, Cantera is used to compute strained flames (twin flame) of the mixtures investigated, where the strained premixed flame is obtained with a counterflow of two streams of fresh gases going against one another, leading to a strained flame (Klimov 1963; Buckmaster and Mikolaitis 1982). The normalized heat release rate of these strained flames is mapped in Fig. 14, where the conditional mean of the 3-D DNS and the unstrained flame speed results are also shown. The strain value of the Cantera flames are 10 , 100 and 1000 s^{-1} . Negative strains cannot be computed with one-dimensional strained flame, and, although compressed flame are expected to have an impact on the broad heat release rate scatter, they cannot be investigated here, and the comparison is limited to positive strain rate. For Cases A, B and C, increasing the strain leads to a higher heat release, whereas the opposite occurs for Case D. This is directly linked to the Markstein number of these flames, which is negative for Cases A, B and C and positive for Case D. This indicates the mixture's sensitivity to strain. Therefore, the scatter of heat release rate in Fig. 5a is due to both the preferential diffusion changing the equivalence ratio and enhanced by curvature effects, and the sensitivity to strain of the mixtures which also affects the heat release rate when preferential diffusion effects are present.

3.2 A Model for Premixed, Turbulent, Thermo-diffusively Unstable NH_3/H_2 Mixtures

Based on the DNS results, this section aims to develop an a priori model for the modeling of turbulent premixed unstable lean ammonia/hydrogen mixtures. This is done in two steps by computing the stretch factor of any mixtures that are considered unstable by strained flames. The first part of this model, however, is to define the scope in which it should be applied. The predictive assessment method is valid for the range of equivalence ratio and mixture fraction investigated here, at ambient conditions of pressure and temperature, and at the range of turbulence investigated in the previous DNS.

3.2.1 Markstein Length

The first part of the predictive tool uses the Markstein number Ma (or length) theories to identify positive or negative values of the Markstein number and to serve as an indicator of the strain sensitivity to the mixture, as already discussed in Sect. 3.1.5. A map of Markstein number isocontour is computed using the theoretical formula (Bechtold and Matalon 2001; Poinso and Veynante 2005; Clavin and Joulin 1983):

$$Ma = \frac{L_b}{\delta_D} = \frac{\beta(Le_{\text{eff}} - 1)}{2(\sigma - 1)} \int_1^\sigma \frac{\bar{\lambda}(x)}{x} \ln \frac{\sigma - 1}{x - 1} dx, \quad (16)$$

where L_b is the Markstein length, β is the Zel'dovich number, Le_{eff} is the effective Lewis number, σ is the expansion ratio, $\delta_D = D_{th}/s_L^0$ is the diffusive flame thickness where D_{th} is the thermal diffusivity and λ is the thermal conductivity. Defined by Joulin and Mitani (Joulin and Mitani 1981) for two reactant flames, and shown to be generalizable by Sun et al. (1999) for complex reactions, Le_{eff} is given by:

$$Le_{\text{eff}} = \begin{cases} \frac{Le_O + ALe_F}{1+A}, A = 1 + \beta(\phi^{-1} - 1) & \text{if } \phi < 1, \\ \frac{Le_F + ALe_O}{1+A}, A = 1 + \beta(\phi - 1) & \text{if } \phi > 1, \end{cases} \quad (17)$$

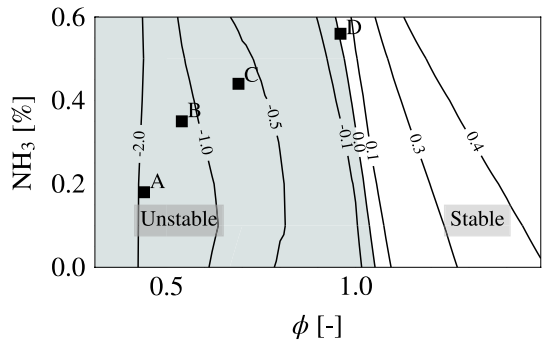
where Le_F and Le_O are the fuel's and oxidant's Lewis numbers. In the case of this study, the Le_F is formulated with a mixture-based definition to account for both fuels. The formula used is proposed by Muppala et al. (2009), who suggested a volume-based formulation of the fuel's Lewis number (Le_V), based on the volume fraction (X_i) of each fuel in the fuel mixture:

$$Le_V = \sum_{n=1}^f X_i Le_i, \quad (18)$$

with f the number of fuels in the fuel mixture. The Markstein definition and volume-based Lewis number definition were both validated in a previous study (Gaucherand et al. 2023). The Markstein number is computed for a range of NH_3/H_2 mixture ranging from 0% of NH_3 to 60% of NH_3 . The equivalence ratio ranges from 0.3 to 1.5, depending on the content of NH_3 since the equivalence ratio lower bound is higher due to the extinction limit. Figure 15 presents the isocontour of computed Markstein values based on the equivalence ratio and NH_3 content in the mixture. The squares correspond to the operating points of the four DNS cases.

Cases A, B and C are, as anticipated, in the negative zone of the Markstein numbers, whereas Case D is very close to 0 but positive. This map provides an evaluation of the

Fig. 15 Isocontour of Markstein number values based on the ratio of NH_3/H_2 and equivalence ratio. The 3-D DNS cases are positioned on the map using the squares



sensitivity to strain to different mixtures. The mixtures on the left of the 0 thresholds are expected to be highly sensitive to the thermo-diffusive effects described before and exhibit high values of stretch factors, such as for Cases A, B and C. Mixtures on the right of the threshold are instead expected to have a stretch factor close to unity, as it is for Case D. Of course, this would need to be validated by a larger amount of operating points, but currently, in the literature, the study of turbulent ammonia/hydrogen flames starting at 1 bar and 300K, and the computation of their stretch factor, is scarce.

If the mixture is stable in the Markstein map, then a unity stretch factor can be considered and no correction to common combustion models is necessary. However, when the mixture is unstable, one should apply a correction for the stretch factor. In the following, we propose a methodology to evaluate the correction with strained flames.

3.2.2 Stretch Factor Derived from Strained Flames

Since the first effect of the Markstein numbers being unstable seems to be the increase of the local laminar flame speed, we show here that this increase is reasonably well captured by simple laminar strained flames. This is further supported by the turbulent flames of the unstable mixtures described in the first part of the discussion section. By modeling the stretch factor effects of complex turbulent flames where thermo-diffusive effects are important with stable 1-D strained flames, one must understand that the 1-D strained flames model is not integrating the entirety of the phenomenon observed in the turbulent flames and discussed before. However, what is suggested here, is that in order to improve modeling of unstable mixtures, a first order approach using the stretch factor from 1-D strained computations would lead to improved results over using $I_0 = 1$. A similar approach as Coulon et al. (2023) is used where the data from a premixed turbulent DNS of lean pure H_2 flame was compared to 1-D strained flames at varying equivalence ratio. The comparison differs in the way that, instead of comparing a large range of strain, the simulations are run at iso-strain of $\approx 2000 \text{ s}^{-1}$ as it is close to the mean value of strain from the DNS data in Fig. 12, and the effects of NH_3 content in the fuel and equivalence ratio are investigated. The iso-contour of s_c/s_L^0 is considered with $s_c = 1/(\rho_u Y_{f,u}) \int_x \dot{\omega}_f dx$ is the consumption speed of the strained flame, and s_L^0 the consumption speed of the unstretched flame at the same composition. Strained flames are computed using Cantera using premixed twin flames. We note here that the previous discussion on the flame description included the importance of curvature in turbulent flames and preferential diffusion. However, by accounting for non-unity Lewis

Fig. 16 Isocontour of the strained derived $I_0^{strained} = s_c/s_L^0$ at $2000s^{-1}$ based on the ratio of NH_3/H_2 and equivalence ratio

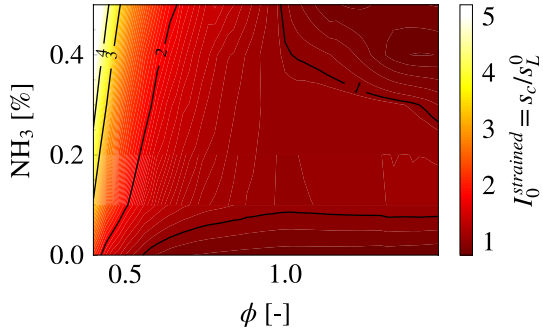


Table 3 Comparison between I_0^{3D} and $I_0^{strained}$ for the four simulations

Case Name	A	B	C	D
I_0^{3D}	2.69	2.16	1.52	1.12
$I_0^{strained}$	2.66	2.18	1.55	0.95

in the transport of species, this should have already been taken into account in simulations. Therefore, a model based on the curvature implications should not be necessary. Furthermore, as the separation of the contribution of the stretch component to the flame speed is a complex ordeal, and no simplified setups (such as the twin flame for the strain) exist for the effects of curvature, a model based on the strain and computed with 1-D strained flames seems to be the most straightforward to account for the stretch factor effects and compute the flame speed acceleration.

Figure 16 presents the results of $I_0^{strained}$ through isocontours of s_c/s_L^0 . Table 3 compares the results between $I_0^{1Dstrained}$ and I_0^{DNS} from Table 2. The comparison is done using the stretch factors in the DNS computed with H_2 , but the results are similar for the NH_3 case.

I_0^{DNS} is well predicted using $I_0^{strained}$ for Cases A, B and C, but not for Case D, validating the use of $I_0^{strained}$ in this a priori model validation of 1-D strained flames as first-order approximations to compute the stretch factor of turbulent unstable mixtures. Regarding Case D, it had a positive Markstein number: the prediction of Fig. 16 using strained flames may only be valid when the Markstein number of a mixture is negative. Of course, integrating a model based on strained flames would require an evaluation the mean flame strain. However, if this is overcome, one can estimate the stretch factor that needs to be accounted for in the ratio of s_T/s_L^0 in flamelet modeling using strained flame for parametrization. Although the present results do not evaluate a flamelet modeling approach, it provides insight in the importance of strained laminar flames for turbulent premixed combustion of ammonia/hydrogen, at least in the thin reaction zone. The stretch factor correction suggested is valid for similar conditions of strain as the 3-D DNS, for the range of equivalence ratio, ammonia content, and turbulent conditions from the DNS.

4 Conclusion

Four Direct Numerical Simulations of premixed turbulent flames with detailed chemistry have been performed, for different equivalence ratios and NH_3/H_2 contents. A progress variable based on H_2O is found to be suited to parametrize the combustion of these mixtures as it reduces the irreducible error the most for the scatter of heat release rate and equivalence ratio. The fuel composition and equivalence ratio are found to substantially impact the enhancement of consumption rate, due to preferential diffusion of light-diffusing species leading to local enrichment and generation of thermo-diffusive effects especially so in lean cases as found from the radical pool. Flames with similar flame speeds have similar strain rates and all flames exhibit different curvature, decreasing with equivalence ratio and H_2 content. Still, the flame's stretch factor differs for each flame, going from unity to more than 2, due to thermo-diffusive effects. Based on the mixture composition, an attempt to discriminate which mixtures are expected to be unstable and have a stretch factor higher than unity is done using the Markstein number as an indicator. This is useful for several purposes. From a modeling point of view, it indicates if a model needs to include thermo-diffusive effects or not. A model accounting for preferential diffusion effects in turbulent flames would be relevant for Cases A, B and C, but a standard flamelet model with unity stretch factor would be sufficient for Case D. One-dimensional strained flames are used to see if the stretch factor can be computed a priori for modeling purposes, and the leanest cases are well predicted by the strained flame velocity increase compared to the unstretched one. The development of this tool can serve both for theoretical modeling, to support the choice of model used, and for practical decision-making of operating points for ammonia/hydrogen mixtures for engine manufacturers.

Supplementary Information The online version contains supplementary material available at <https://doi.org/10.1007/s10494-023-00515-1>.

Acknowledgements Computations were performed partly on resources provided by Sigma2 - the National Infrastructure for High-Performance Computing and Data Storage in Norway (project nn9527k), on the BETZY supercomputer, and of GENCI-TGCC under grant agreement n° 2024-A0152B10157. CERFACS provided the software AVBP, and technical support for the software was provided by Dr. O. Vermorel and Dr. G. Staffelbach. Dr. A. Gruber is also acknowledged for providing computational resources and technical support. Mr. A. Hasan is also acknowledged for the help provided for the archiving of the data.

Author Contributions JG set up and performed the DNSs, the post-processing of the DNS and of one-dimensional flames to support the analysis, and wrote the paper. CSN contributed to the post-processing of some of the data. The study was designed and guided by TP, CSN and DL. All the co-authors contributed to analyzing the results and reviewing the paper.

Funding Open access funding provided by NTNU Norwegian University of Science and Technology (incl St. Olavs Hospital - Trondheim University Hospital). The Authors gratefully acknowledge the support from the Norwegian Research Council (296207) and related partners in the Low Emission Centre. This project has received funding from the European Research Council under the European Union's Horizon 2020 research and innovation program Grant Agreement 832248, SCIROCCO.

Data Availability The DNS data that support the findings of this study are made available with the help of Sigma2 archiving system, at the following address: <https://doi.org/10.11582/2023.00010> (Gaucherand 2023). The mesh information, initial solutions and the solutions files with information such as the heat release, temperature, species mass fraction and other variables, at different time steps are available.

Declaration

Conflict of interest The authors declare that they have no known competing financial interests or personal relationships that could have appeared to influence the work reported in this paper.

Open Access This article is licensed under a Creative Commons Attribution 4.0 International License, which permits use, sharing, adaptation, distribution and reproduction in any medium or format, as long as you give appropriate credit to the original author(s) and the source, provide a link to the Creative Commons licence, and indicate if changes were made. The images or other third party material in this article are included in the article's Creative Commons licence, unless indicated otherwise in a credit line to the material. If material is not included in the article's Creative Commons licence and your intended use is not permitted by statutory regulation or exceeds the permitted use, you will need to obtain permission directly from the copyright holder. To view a copy of this licence, visit <http://creativecommons.org/licenses/by/4.0/>.

References

- Aniello, A., Laera, D., Berger, L., Attili, A., Poinso, T.: Introducing thermodiffusive effects in large-eddy simulation of turbulent combustion for lean hydrogen-air flames. (2022)
- Aspden, A., Day, M., Bell, J.: Turbulence-chemistry interaction in lean premixed hydrogen combustion. *Proc. Comb. Inst.* **35**, 1321–1329 (2015). <https://doi.org/10.1016/j.proci.2014.08.012>
- Barenblatt, G.: On diffusive-thermal stability of a laminar flame. *J. Appl. Mech. Tech. Phys.* **4**, 21–26 (1962)
- Bechtold, J., Matalon, M.: The dependence of the markstein length on stoichiometry. *Combust. Flame* **127**, 1906–1913 (2001). [https://doi.org/10.1016/S0010-2180\(01\)00297-8](https://doi.org/10.1016/S0010-2180(01)00297-8)
- Berger, L., Attili, A., Pitsch, H.: Intrinsic instabilities in premixed hydrogen flames: Parametric variation of pressure, equivalence ratio, and temperature. Part 1 - dispersion relations in the linear regime. *Combust. Flame* **240**, 111935 (2022). <https://doi.org/10.1016/j.combustflame.2021.111935>
- Berger, L., Attili, A., Pitsch, H.: Intrinsic instabilities in premixed hydrogen flames: parametric variation of pressure, equivalence ratio, and temperature. part 2 “non” linear regime and flame speed enhancement. *Combust. Flame* **240**, 111936 (2022). <https://doi.org/10.1016/j.combustflame.2021.111936>
- Berger, L., Attili, A., Pitsch, H.: Synergistic interactions of thermodiffusive instabilities and turbulence in lean hydrogen flames. *Combust. Flame* **244**, 112254 (2022). <https://doi.org/10.1016/j.combustflame.2022.112254>
- Berger, L., Kleinheinz, K., Attili, A., Pitsch, H.: Characteristic patterns of thermodiffusively unstable premixed lean hydrogen flames. *Proc. Comb. Inst.* **37**, 1879–1886 (2019). <https://doi.org/10.1016/j.proci.2018.06.072>
- Bilger, R., Stårner, S., Kee, R.: On reduced mechanisms for methane-air combustion in nonpremixed flames. *Combust. Flame* **80**, 135–149 (1990). [https://doi.org/10.1016/0010-2180\(90\)90122-8](https://doi.org/10.1016/0010-2180(90)90122-8)
- Borghini, R.: On the structure and morphology of turbulent premixed flames, *Recent Adv. Aerosp. Sci.* 117–138 (1985)
- Böttler, H., Lulic, H., Steinhausen, M., Wen, X., Hasse, C., Scholtissek, A.: Flamelet modeling of thermo-diffusively unstable hydrogen-air flames. *Proc. Comb. Inst.* (2023). <https://doi.org/10.1016/j.proci.2022.07.159>
- Buckmaster, J., Mikolaitis, D.: The premixed flame in a counterflow. *Combust. Flame* **47**, 191–204 (1982). [https://doi.org/10.1016/0010-2180\(82\)90100-6](https://doi.org/10.1016/0010-2180(82)90100-6)
- Cazères, Q., Pepiot, P., Riber, E., Cuenot, B.: A fully automatic procedure for the analytical reduction of chemical kinetics mechanisms for computational fluid dynamics applications. *Fuel* **303**, 121247 (2021). <https://doi.org/10.1016/j.fuel.2021.121247>
- Chi, C., Han, W., Thévenin, D.: Effects of molecular diffusion modeling on turbulent premixed ammonia/hydrogen/air flames. *Proc. Comb. Inst.* **39**, 2259–2268 (2023). <https://doi.org/10.1016/j.proci.2022.08.074>
- Clavin, P., Joulin, G.: Premixed flames in large scale and high intensity turbulent flow. *J. Phys. Lett.* (1983). <https://doi.org/10.1051/jphyslet:019830044010100>
- Colin, O., Rudgyard, M.: Development of high-order taylor-galerkin schemes for LES. *J. Comput. Phys.* (2000). <https://doi.org/10.1006/jcph.2000.6538>
- Coulon, V., Gaucherand, J., Xing, V., Laera, D., Lapeyre, C., Poinso, T.: Direct numerical simulations of methane, ammonia-hydrogen and hydrogen turbulent premixed flames. *Combust. Flame* **256**, 112933 (2023). <https://doi.org/10.1016/j.combustflame.2023.112933>

- Darrieus, G.: Propagation d'un front de flamme. *La Technique Moderne* **30**, 18 (1938)
- Domingo, P., Vervisch, L.: Recent developments in DNS of turbulent combustion. *Proc. Comb. Inst.* **39**, 2055–2076 (2022). <https://doi.org/10.1016/j.proci.2022.06.030>
- Echehki, T., Chen, J.H.: Analysis of the contribution of curvature to premixed flame propagation. *Combust. Flame* **144**, 492–497 (1999). [https://doi.org/10.1016/S0010-2180\(99\)00006-1](https://doi.org/10.1016/S0010-2180(99)00006-1)
- Gaucherand, J.: Direct numerical simulation premixed turbulent flame, (2023). <https://doi.org/10.11582/2023.00010>
- Gaucherand, J., Laera, D., Schulze-Netzer, C., Poinso, T.: Intrinsic instabilities of hydrogen and hydrogen/ammonia premixed flames: influence of equivalence ratio, fuel composition and pressure. *Combust. Flame* **256**, 112986 (2023). <https://doi.org/10.1016/j.combustflame.2023.112986>
- Goodwin, D.G., Moffat, H.K., Schoegl, I., Speth, R.L., Weber, B.W.: Cantera: an object-oriented software toolkit for chemical kinetics, thermodynamics, and transport processes. Version 2.6.0 (2022)
- Gran, I.R., Echehki, T., Chen, J.H.: Negative flame speed in an unsteady 2D premixed flame: a computational study. *Symp. Combust.* **26**, 323–329 (1996). [https://doi.org/10.1016/S0082-0784\(96\)80232-3](https://doi.org/10.1016/S0082-0784(96)80232-3)
- Hochgreb, S.: How fast can we burn, 2.0. *Procee. Combust. Inst.* **39**, 2077–2105 (2023). <https://doi.org/10.1016/j.proci.2022.06.029>
- Howarth, T., Aspden, A.: An empirical characteristic scaling model for freely-propagating lean premixed hydrogen flames. *Combust. Flame* **237**, 111805 (2022). <https://doi.org/10.1016/j.combustflame.2021.111805>
- Howarth, T., Hunt, E., Aspden, A.: Thermodiffusively-unstable lean premixed hydrogen flames: Phenomenology, empirical modelling, and thermal leading points. *Combust. Flame* **253**, 112811 (2023). <https://doi.org/10.1016/j.combustflame.2023.112811>
- Ichikawa, A., Hayakawa, A., Kitagawa, Y., Somarathne, K.K.A., Kudo, T., Kobayashi, H.: Science and technology of ammonia combustion. *Proc. Comb. Inst.* **37**, 109–133 (2019). <https://doi.org/10.1016/j.ijhydene.2015.04.024>
- Ihme, M., Shunn, L., Zhang, J.: Regularization of reaction progress variable for application to flamelet-based combustion models. *J. Comput. Phys.* **231**, 7715–7721 (2012). <https://doi.org/10.1016/j.jcp.2012.06.029>
- Im, H.G., Chen, J.H.: Preferential diffusion effects on the burning rate of interacting turbulent premixed hydrogen-air flames. *Combust. Flame* **131**, 246–258 (2002). [https://doi.org/10.1016/S0010-2180\(02\)00405-4](https://doi.org/10.1016/S0010-2180(02)00405-4)
- Joulin, G., Mitani, T.: Linear stability analysis of two-reactant flames. *Combust. Flame* **40**, 235–246 (1981). [https://doi.org/10.1016/0010-2180\(81\)90127-9](https://doi.org/10.1016/0010-2180(81)90127-9)
- Karimkashi, S., Tamadonfar, P., Kaario, O., Vuorinen, V.: A numerical investigation on effects of hydrogen enrichment and turbulence on NO formation pathways in premixed ammonia/air flames. *Combust. Sci. Technol.* (2023). <https://doi.org/10.1080/00102202.2023.2180634>
- Klimov, A.: Laminar flame in a turbulent flow, *Prikladnoy Mekhaniki i Tekhnicheskoy Fiziki Zhurnal*, (USSR) (1963) 49–58
- Knop, V., Michel, J.-B., Colin, O.: On the use of a tabulation approach to model auto-ignition during flame propagation in SI engines. *Appl. Energy* **88**, 4968–4979 (2011). <https://doi.org/10.1016/j.apenergy.2011.06.047>
- Kraichnan, R.H.: Diffusion by a random velocity field. *Phys. Fluids* **13**, 22–31 (1970). <https://doi.org/10.1063/1.1692799>
- Kuenne, G., Ketelheun, A., Janicka, J.: LES modeling of premixed combustion using a thickened flame approach coupled with FGM tabulated chemistry. *Combust. Flame* **158**, 1750–1767 (2011). <https://doi.org/10.1016/j.combustflame.2011.01.005>
- Landau, L.: On the theory of slow combustion. In: Pelcé, P. (ed.) *Dynamics of Curved Fronts*, pp. 403–411. Academic Press, San Diego (1988). <https://doi.org/10.1016/B978-0-08-092523-3.50044-7>
- Lee, H.C., Dai, P., Wan, M., Lipatnikov, A.N.: Lewis number and preferential diffusion effects in lean hydrogen-air highly turbulent flames. *Phys. Fluids* **34**, 035131 (2022). <https://doi.org/10.1063/5.0087426>
- Lehtiniemi, H., Mauss, F., Balhasar, M., Magnusson, L.: Modeling diesel spray ignition using detailed chemistry with a progress variable approach. *Combust Sci Technol.* **178**, 1977–1997 (2006). <https://doi.org/10.1080/00102200600793148>
- Lipatnikov, A., Chomiak, J.: Molecular transport effects on turbulent flame propagation and structure. *Prog. Energy Combust. Sci.* **31**, 1–73 (2005). <https://doi.org/10.1016/j.pecs.2004.07.001>
- Luca, S., Attili, A., Schiavo, E.L., Creta, F., Bisetti, F.: On the statistics of flame stretch in turbulent premixed jet flames in the thin reaction zone regime at varying reynolds number. *Proc. Comb. Inst.* **37**, 2451–2459 (2019). <https://doi.org/10.1016/j.proci.2018.06.194>
- MacFarlane, D.R., Cherepanov, P.V., Choi, J., Suryanto, B.H., Hodgetts, R.Y., Bakker, J.M., Ferrero Vallana, F.M., Simonov, A.N.: A roadmap to the ammonia economy. *Joule* **4**, 1186–1205 (2020). <https://doi.org/10.1016/j.joule.2020.04.004>

- Matalon, M.: Intrinsic flame instabilities in premixed and nonpremixed combustion. *Annu. Rev. Fluid Mech.* **39**, 163–191 (2007). <https://doi.org/10.1146/annurev.fluid.38.050304.092153>
- Mukundakumar, N., Bastiaans, R.: DNS study of spherically expanding premixed turbulent ammonia-hydrogen flame kernels, effect of equivalence ratio and hydrogen content. *Energies* (2022). <https://doi.org/10.3390/en15134749>
- Muppala, S., Nakahara, M., Aluri, N., Kido, H., Wen, J., Papalexandris, M.: Experimental and analytical investigation of the turbulent burning velocity of two-component fuel mixtures of hydrogen, methane and propane. *Int. J. Hydrog. Energy* **34**, 9258–9265 (2009). <https://doi.org/10.1016/j.ijhydene.2009.09.036>
- Netzer, C., Ahmed, A., Gruber, A., Lövås, T.: Curvature effects on NO formation in wrinkled laminar ammonia/hydrogen/nitrogen-air premixed flames. *Combust. Flame* **232**, 111520 (2021). <https://doi.org/10.1016/j.combustflame.2021.111520>
- Niu, Y.-S., Vervisch, L., Tao, P.D.: An optimization-based approach to detailed chemistry tabulation: automated progress variable definition. *Proc. Comb. Inst.* **160**, 776–785 (2013). <https://doi.org/10.1016/j.combustflame.2012.11.015>
- Oijen, V., Bastiaans, R.R., Goey, D.: Modelling preferential diffusion effects in premixed methane-hydrogen-air flames by using flamelet-generated manifolds, in: *ECCOMASCFD2010*, (2010)
- Orszag, S.A.: Analytical theories of turbulence. *J. Fluid Mech.* **41**, 363–386 (1970). <https://doi.org/10.1017/S0022112070000642>
- Passot, T., Pouquet, A.: Numerical simulation of compressible homogeneous flows in the turbulent regime. *J. Fluid Mech.* **181**, 441–466 (1987). <https://doi.org/10.1017/S0022112087002167>
- Peters, N.: *Turbulent Combustion*. Cambridge University Press, Cambridge (2000)
- Peters, N., Terhoeven, P., Chen, J.H., Echehki, T.: Statistics of flame displacement speeds from computations of 2D unsteady methane-air flames. *Symp. Combust.* **27**, 833–839 (1998). [https://doi.org/10.1016/S0082-0784\(98\)80479-7](https://doi.org/10.1016/S0082-0784(98)80479-7)
- Pierce, C.D., Moin, P.: Progress-variable approach for large-eddy simulation of non-premixed turbulent combustion. *J. Fluid Mech.* **504**, 73–97 (2004). <https://doi.org/10.1017/S0022112004008213>
- Poinsot, T., Lele, S.: Boundary conditions for direct simulations of compressible viscous flows. *J. Comput. Phys.* **101**, 104–129 (1992). [https://doi.org/10.1016/0021-9991\(92\)90046-2](https://doi.org/10.1016/0021-9991(92)90046-2)
- Poinsot, T., Veynante, D.: *Theoretical and numerical combustion*, RT Edwards, Inc., (2005)
- Pope, S.B.: The evolution of surfaces in turbulence. *Int. J. Eng. Sci.* **26**, 445–469 (1988)
- Prüfer, U., Hartl, S., Hunger, F., Messig, D., Eiermann, M., Hasse, C.: A constrained control approach for the automated choice of an optimal progress variable for chemistry tabulation. *Flow Turbul. Combust.* **94**, 593–617 (2015). <https://doi.org/10.1007/s10494-015-9595-3>
- Rieth, M., Gruber, A., Chen, J.H.: The effect of pressure on lean premixed hydrogen-air flames. *Combust. Flame* **250**, 112514 (2023). <https://doi.org/10.1016/j.combustflame.2022.112514>
- Rieth, M., Gruber, A., Williams, F.A., Chen, J.H.: Enhanced burning rates in hydrogen-enriched turbulent premixed flames by diffusion of molecular and atomic hydrogen. *Combust. Flame* **239**, 111740 (2022). <https://doi.org/10.1016/j.combustflame.2021.111740>
- Rogallo, R.S., Moin, P.: Numerical simulation of turbulent flows. *Annu. Rev. Fluid Mech.* **16**, 99–137 (1984). <https://doi.org/10.1146/annurev.fl.16.010184.000531>
- Schönfeld, T., Rudgyard, M.: Steady and unsteady flow simulations using the hybrid flow solver avbp. *AIAA* **37**, 1378–1385 (1999). <https://doi.org/10.2514/2.636>
- Song, W., Hernández-Pérez, F.E., Im, H.G.: Diffusive effects of hydrogen on pressurized lean turbulent hydrogen-air premixed flames. *Combust. Flame* **246**, 112423 (2022). <https://doi.org/10.1016/j.combustflame.2022.112423>
- Staffell, I., Scamman, D., Velazquez Abad, A., Balcombe, P., Dodds, P.E., Ekins, P., Shah, N., Ward, K.R.: The role of hydrogen and fuel cells in the global energy system. *Energy Environ. Sci.* **12**, 463–491 (2019). <https://doi.org/10.1039/C8EE01157E>
- Stagni, A., Cavallotti, C., Arunthanayothin, S., Song, Y., Herbinet, O., Battin-Leclerc, F., Faravelli, T.: An experimental, theoretical and kinetic-modeling study of the gas-phase oxidation of ammonia, *React. Chem. Eng.* **5**, 696–711 (2020). <https://doi.org/10.1039/C9RE00429G>
- Sun, C., Sung, C., He, L., Law, C.: Dynamics of weakly stretched flames: quantitative description and extraction of global flame parameters. *Combust. Flame* **118**, 108–128 (1999). [https://doi.org/10.1016/S0010-2180\(98\)00137-0](https://doi.org/10.1016/S0010-2180(98)00137-0)
- Valera-Medina, A., Amer-Hatem, F., Azad, A.K., Dedoussi, I.C., de Joannon, M., Fernandes, R.X., Glarborg, P., Hashemi, H., He, X., Mashruk, S., McGowan, J., Mounaim-Rousellet, C., Ortiz-Prado, A., Ortiz-Valera, A., Rossetti, I., Shu, B., Yehia, M., Xiao, H., Costa, M.: Review on ammonia as a potential fuel: from synthesis to economics. *Eng. Fuel* **35**, 6964–7029 (2021). <https://doi.org/10.1021/acs.energyfuels.0c03685>

- Wiseman, S., Rieth, M., Gruber, A., Dawson, J.R., Chen, J.H.: A comparison of the blow-out behavior of turbulent premixed ammonia/hydrogen/nitrogen-air and methane-air flames. *Proc. Comb. Inst.* **38**, 2869–2876 (2021). <https://doi.org/10.1016/j.proci.2020.07.011>
- Yang, W., Ranga Dinesh, K., Luo, K., Thevenin, D.: Direct numerical simulation of turbulent premixed ammonia and ammonia-hydrogen combustion under engine-relevant conditions. *Int. J. Hydrog. Energy* **47**, 11083–11100 (2022). <https://doi.org/10.1016/j.ijhydene.2022.01.142>
- Zhang, W., Karaca, S., Wang, J., Huang, Z., van Oijen, J.: Large eddy simulation of the Cambridge/Sandia stratified flame with flamelet-generated manifolds: Effects of non-unity Lewis numbers and stretch. *Combust. Flame* **227**, 106–119 (2021). <https://doi.org/10.1016/j.combustflame.2021.01.004>